J|A|C|S ARTICLES

Published on Web 10/15/2009

Modified Thermodynamics in Ionic Liquids for Controlled Electrocrystallization of Nanocubes, Nanowires, and Crystalline Thin Films of Silver−Tetracyanoquinodimethane

Chuan Zhao, Douglas R. MacFarlane, and Alan M. Bond*

School of Chemistry and ARC Special Research Centre for Green Chemistry, Monash University, Clayton, Victoria 3800, Australia

Received July 29, 2009; E-mail: alan.bond@sci.monash.edu.au

Abstract: Electrocrystallization of nanocubes, nanorods, nanowires, and crystalline thin films of silver−tetracyanoquinodimethane (AgTCNQ) onto glassy carbon, indium tin oxide, and platinum electrodes can be achieved from ionic liquids containing dissolved TCNQ and Ag(I) salts. In conventional molecular organic solvents, such as acetonitrile, the reduction of TCNQ and Ag^+ occurs at almost the same potential. In contrast, the different thermodynamics that apply to the room temperature ionic liquid, 1-*n*-butyl-3-methylimidazolium tetrafluoroborate ($BMIMBF_4$), give rise to a large potential separation in the two processes, which enables electrocrystallization of AgTCNQ to be undertaken via two distinctly different, potential-dependent mechanisms. Cyclic and microelectrode voltammetric, chronoamperometric, together with microscopic and spectroscopic techniques reveal that AgTCNQ nanostuctures of controlled morphology, size, density, and uniformity can be achieved by tuning the electrocrystallization parameters such as potential, stoichiometric ratio of Ag^+ and TCNQ, and their concentrations, time, and ionic liquid viscosity by altering the water content. In the potential range of −0.1 to 0.3 V vs $Fc^{0/+}$ (Fc = ferrocene), electrocrystallization occurs when Ag is deposited at electrode defect sites via a progressive nucleation and 3-D growth mechanism followed by reaction with TCNQ to produce structures ranging from nanocubes to nanowires. At higher stoichiometric concentrations of Ag^+ and more negative potentials (<−0.1 V vs $Fc^{0/+}$), extremely thin crystalline films could be obtained via overpotential deposition. Infrared and Raman spectroscopy, elemental analysis, together with X-ray diffraction and scanning electron microscopy all confirm the formation of highly pure AgTCNQ nanomaterials, which exhibit differences in morphology but not phase. The study highlights the capability of the electrocrystallization method to precisely control the morphology of nanomaterials, and also the unprecedented opportunities provided by using ionic liquids as the medium for preparation of technologically important metal−TCNQ charge transfer complexes.

Introduction

Down-scaling the size of flash and dynamic random access memory (RAM) is becoming more and more challenging as the physical limits for the storage mechanism are approached, and the required processing technology becomes more complex.[1,2] Memories made from metal−oxide electrical switching materials, phase change charge transfer materials, and organic semiconducting polymers appear to be alternative contenders to succeed flash memory and for enlarging the capabilities of nonvolatile memory.[1−4] Memories based on these materials can be further down-scaled by incorporating resistive-switching nanowires as memory elements in interconnects via substrate structures.[4] Various metal salts of tetracyanoquinodimethane (TCNQ) represent complexes that exhibit a range of intriguing electronic, optical, and magnetic effects.[5−14] AgTCNQ, together with CuTCNQ, have attracted particular attention because they exhibit high structural flexibility, and reproducible nanosecond electrical and optical switching behavior and memory effects, making them excellent candidates for use in molecular electronics and sensors.[5−12] Induced by an electric field or optical excitation, AgTCNQ can undergo reversible and bistable switching of conductivity from a low to a high state (eq 1) due to the π-orbital overlapping of neighboring molecules.[13,14]

(1) Atwood, G. *Science* **2008**, *321*, 210–211.
(2) Bez, R.; Pirovano, A. *Mater. Sci. Semicond. Process.* **2004**, *7*, 349.
(3) Wuttig, M. *Nat. Mater.* **2005**, *4*, 265–266.
(4) Müller, R.; De Jonge, S.; Myny, K.; Wouters, D. J.; Genoe, J.; Heremans, P. *Appl. Phys. Lett.* **2006**, *89*, 223501.
(5) Fan, Z.; Mo, X.; Lou, C.; Yao, Y.; Wang, D.; Chen, G.; Lu, J. *IEEE Trans. Nanotechnol.* **2005**, *4*, 238.
(6) Oyamada, T.; Tanaka, H.; Matsushige, K.; Sasabe, H.; Adachi, C. *Appl. Phys. Lett.* **2003**, *83*, 1252.
(7) Liu, H.; Zhao, Q.; Li, Y.; Liu, Y.; Lu, F.; Zhuang, J.; Wang, S.; Jiang, L.; Zhu, D.; Yu, D.; Chi, L. *J. Am. Chem. Soc.* **2005**, *127*, 1120.
(8) Cao, G.; Ye, C.; Fang, F.; Xing, X.; Xu, H.; Sun, D.; Chen, G. *Mater. Sci. Eng., B* **2005**, *119*, 41.
(9) Liu, Y. L.; Ji, Z. Y.; Tang, Q. X.; Jiang, L.; Li, H. X.; He, M.; Hu, W. P.; Zhang, D. Q.; Wang, X. K.; Wang, C.; Liu, Y. Q.; Zhu, D. B. *Adv. Mater.* **2005**, *17*, 2953.
(10) Muller, R.; Genoe, J.; Heremans, P. *Appl. Phys. Lett.* **2006**, *88*, 103501.
(11) Muller, R.; De Jonge, S.; Myny, K.; Wouters, D. J.; Genoe, J.; Heremans, P. *Solid-State Electron.* **2006**, *50*, 602.
(12) Xiao, K.; Tao, J.; Pan, Z.; Puretzky, A. A.; Ivanov, I. N.; Pennycook, S. J.; Geohegan, D. B. *Angew. Chem., Int. Ed.* **2007**, *46*, 2650.
(13) Potember, R. S.; Poehler, T. O.; Cowan, D. O. *Appl. Phys. Lett.* **1979**, *34*, 405.
(14) Kamitsos, E. I.; Risen, J. W. M. *Solid State Commun.* **1983**, *45*, 165.

$$[M^+TCNQ^-]_n \text{ ``OFF'' state} \xrightarrow{\text{voltage}} M_x^0 + TCNQ_x^0 + \underset{\text{``ON'' state}}{[M^+TCNQ^-]_{n-x}} \quad (M = Ag, Cu;\ 0 < x < n) \tag{1}$$

Fostered by interest in molecular switching and memory storage devices, a diverse range of techniques have been introduced to achieve precise control of the morphology and phase, structure, and purity of AgTCNQ and CuTCNQ materials. These include spontaneous electrolysis (reaction between dissolved TCNQ in acetonitrile and metallic Ag or Cu),[8,9,15] vacuum vapor deposition of TCNQ onto metal surfaces at low temperature,[14,16] thermal vapor deposition of TCNQ on Ag at 150−180 °C,[17] reactions in organic solvents using TCNQ and metal salt precursors,[18] and photoreduction of TCNQ in presence of Ag^+.[19] Of all of the techniques used in the synthesis of AgTCNQ, which is the material of interest in this study, electrocrystallization is one of the most versatile. Importantly, it enables precise control of the nucleation and growth processes, and the purity, structure, and morphologies of the crystals, and often operates under ambient and benign conditions.

Early studies based on electrocrystallization of AgTCNQ employed polarized Ag electrodes in acetonitrile containing TCNQ, or electrocrystallization of AgTCNQ on Ag substrates by oxidation of silver anodes in acetonitrile solutions containing a $TCNQ^-$ (LiTCNQ) salt.[20,21] Recent contributions from this laboratory have focused on controlled potential methods for electrocrystallization of metal−TCNQ materials onto electrode surfaces from acetonitrile using electroreduction of TCNQ in the presence of metal salt precursors, or from aqueous solutions using solid−solid electrochemical transformation of microparticles of TCNQ adhered to an electrode in contact with a metal salt electrolyte.[22−28] In the case of Cu, Co, Ni, and Fe−TCNQ complexes, these approaches have provided significant insights into the nucleation−growth process and allowed control of the morphology and even phase.[25−28] However, the electrocrystallization of AgTCNQ from a molecular solvent has been less successful because the reduction of both TCNQ and Ag^+ occurs at almost the same potential in acetontrile (230 mV vs Ag/AgCl) and in aqueous media, so that the potential window available for control of electrocrystallization is very restricted.[24]

In view of limitations encountered in conventional media, we have developed a facile and reproducible approach using ionic liquids for controlled electrocrystallization of AgTCNQ nanocubes, nanowires, and crystalline thin films onto carbon, metal, and semiconducting electrode surfaces. Ionic liquids (ILs) have proven to be particularly attractive media for electrodeposition because of a large electrochemical potential window, high solubility of metal salts, avoidance of deleterious water and water/metal reactions, intrinsically high conductivity, low interfacial tension, which normally results in high nucleation rates and generally smaller nanoparticles, and other features.[29−37] In the present case, we show that the modified thermodynamics available in the ionic liquid $BMIMBF_4$ gives rise to a large potential separation (>400 mV) in the Ag^+ and TCNQ reduction processes, which allows electrocrystallization of AgTCNQ to occur via two distinctly different nucleation−growth mechanisms. Furthermore, the viscosity may be controlled by alteration of the water concentration, allowing the rate of crystal growth to be varied. The unprecedented control over the crystallization processes and morphologies allows nanocubes, nanorods, nanowires, and crystalline thin film AgTCNQ nanostructures to be generated in a controlled manner for the first time under benign room temperature conditions, as required for low-cost flexible electronic applications. Importantly, the nanostructures can be produced at the size needed for down-scaling AgTCNQ-based nonvolatile memory devices. To the best of our knowledge, this is the first use of ionic liquid media for electrocrystallization of the metal−TCNQ class of technologically important materials with controlled morphologies.

Experimental Section

Materials and Chemicals. High purity, 1-*n*-butyl-3-methylimidazolium tetrafluoroborate ($BMIMBF_4$) from Merck, 98% tetrakis(acetonitrile) silver(I) tetrafluoroborate ($Ag(MeCN)_4BF_4$) and silver(I) tetrafluoroborate ($AgBF_4$) from Sigma, ferrocene ($Fe(C_5H_5)_2$ or Fc) from BDH, and 98% 7,7,8,8-tetracyanoquinodimethane (TCNQ) from Sigma were used as provided by the manufacturer.

Electrochemical Procedures. All voltammetric experiments were undertaken at 20 ± 2 °C with a BAS 100B/W Electrochemical Analyzer (Bioanalytical System, West Lafayette, IN) using a standard three-electrode cell arrangement. Glassy carbon (GC) or Pt macrodisc electrodes (Cypress Systems, Lawrence, KS), which have electrode areas of 0.0299 and 0.0134 cm^2, respectively, or a 2 μm diameter Pt microelectrode were used as working electrodes. Prior to each experiment, they were polished with 0.3 μm alumina (Buehler, Lake Bluff, IL) on a clean polishing cloth (Buehler), sequentially rinsed with distilled water and acetone, and finally dried with lint-free tissue paper. Indium tin oxide (ITO) (Prazisions Glas and Optik GmbH, 10 Ω/□ sheet resistance) also was used as a working electrode after cleaning by sonication in acetone for 10 min, rinsing with absolute ethanol, and drying under an N_2 stream.

(15) Heintz, R. A.; Zhao, H.; Ouyang, X.; Grandinetti, G.; Cowen, J.; Dunbar, K. R. *Inorg. Chem.* **1999**, *38*, 144.
(16) Ye, C. N.; Cao, G. Y.; Mo, X. L.; Fang, F.; Xing, X. Y.; Chen, G. R.; Sun, D. L. *Chin. Phys. Lett.* **2004**, *21*, 1787.
(17) Xiao, K.; Tao, J.; Puretzky, A. A.; Ivanov, I. N.; Retterer, S. T.; Pennycook, S. J.; Geohegan, D. B. *Adv. Funct. Mater.* **2008**, *18*, 3043.
(18) O'Kane, S. A.; Clerac, R.; Zhao, H.; Ouyang, X.; Galan-Mascaros, J. R.; Heintz, R.; Dunbar, K. R. *J. Solid State Chem.* **2000**, *152*, 159.
(19) Zhao, C.; Bond, A. M. *J. Am. Chem. Soc.* **2009**, *131*, 4279.
(20) Kathirgamanathan, P.; Rosseinsky, D. R. *J. Chem. Soc., Chem. Commun.* **1980**, 839.
(21) Shields, L. *J. Chem. Soc., Faraday Trans. 2* **1985**, *81*, 1.
(22) Harris, A. R.; Neufeld, A. K.; O'Mullane, A. P.; Bond, A. M.; Morrison, R. J. S. *J. Electrochem. Soc.* **2005**, *152*, C577.
(23) Neufeld, A. K.; Madsen, I.; Bond, A. M.; Hogan, C. F. *Chem. Mater.* **2003**, *15*, 3573.
(24) Harris, A. R.; Nafady, A.; O'Mullane, A. P.; Bond, A. M. *Chem. Mater.* **2007**, *19*, 5499.
(25) Harris, A. R.; Neufeld, A. K.; O'Mullane, A. P.; Bond, A. M. *J. Mater. Chem.* **2006**, *16*, 4397.
(26) Qu, X.; Nafady, A.; Mechler, A.; Zhang, J.; Harris, A. R.; Martin, L. L.; O'Mullane, A. P.; Bond, A. M. *J. Solid-State Electrochem.* **2008**, *12*, 739.
(27) Nafady, A.; Bond, A. M.; Bilyk, A.; Harris, A. R.; Bhatt, A. I.; O'Mullane, A. P.; De Marco, R. *J. Am. Chem. Soc.* **2007**, *129*, 2369.
(28) Nafady, A.; Bond, A. M.; Bilyk, A. *J. Phys. Chem. C* **2008**, *112*, 6700.
(29) Welton, T. *Chem. Rev.* **1999**, *99*, 2071–2084.
(30) Rogers, R. D., Seddon, K. R., Volkov, S., Eds. *Green Industrial Applications of Ionic Liquids*; Kluwer Academic: Dordrecht, Netherlands, 2003.
(31) Zhao, C.; Burrell, G.; Torriero, A. A. J.; Separovic, F.; Dunlop, N. F.; MacFarlane, D.; Bond, A. M. *J. Phys. Chem. B* **2008**, *112*, 6923.
(32) Endres, F.; Abbott, A.; MacFarlane, D. *Electrodeposition from Ionic Liquids*; John Wiley & Sons: Hoboken, NJ, 2008.
(33) Abbott, A. P.; McKenzie, K. J. *Phys. Chem. Chem. Phys.* **2006**, *8*, 4265–4279.
(34) Antonietti, M.; Kuang, D.; Smarsly, B.; Zhou, Y. *Angew. Chem., Int. Ed.* **2004**, *43*, 4988.
(35) Mele, A.; Tran, C. D.; De Paoli Lacerda, S. H. *Angew. Chem., Int. Ed.* **2003**, *42*, 4364.
(36) Fei, Z.; Geldbach, T. J.; Zhao, D.; Dyson, P. J. *Chem.-Eur. J.* **2006**, *12*, 2122.
(37) Itoh, H.; Naka, K.; Chujo, Y. *J. Am. Chem. Soc.* **2004**, *126*, 3026.

A Pt wire was used as the counter electrode. A Ag wire sealed in a glass tube containing $BMIMBF_4$ with a glass frit separating it from the test solution was used as a quasi-reference electrode. The potential of the reference electrode potential was calibrated against the IUPAC recommended internal reference $Fc^{0/+}$ process,[38] to which all potentials are referred.

Physical Characterization Procedures. The water content of $BMIMBF_4$ was determined by Karl Fischer titration (831 KF Coulometer, Metrohm). Scanning electron microscopy (SEM) measurements were achieved with a JEOL 6300F field emission gun (FEG) scanning electron microscope having a WinEDS energy dispersive X-ray (EDAX) analysis accessory. All AgTCNQ samples including those electrocrystallized onto GC or ITO electrode substrates were sputter coated with 10 nm Pt (Dynavac SC150 sputter coater) before the images were collected to increase the production of secondary electrons and hence improve the image quality. Powder X-ray diffraction (XRD) patterns of AgTCNQ electrocrystallized onto an ITO electrode (solvent removed, washed, and dried) were collected at 40 kV and 25 mA using a Phillips 1729 X-ray diffractrometer (XRD) with Cu KR radiation in the range from 2° to 60° 2θ in steps of 0.02° with a counting time of 2 s $step^{-1}$. Infrared spectra were obtained with a Bruker IFS Equinox Fourier transform IR system equipped with a Golden GateTM single bounce diamond Micro-ATR (attenuated total reflectance) cell. Raman spectra were measured with a Renishaw RM 2000 Raman spectrograph and microscope using a laser strength of 18 mW at a wavelength of 780 nm.

Results and Discussion

1. Voltammetric Reduction of TCNQ in "Wet" $BMIMBF_4$ in the Absence of Ag^+. The room temperature ionic liquid $BMIMBF_4$ was chosen for use in this study because of the much higher solubility of TCNQ than that found in other ionic liquids. $BMIMBF_4$ is highly hygroscopic and fully miscible with water at temperatures above 5 °C. Systematic studies have shown that "dried" $BMIMBF_4$ can absorb water from the gas phase to achieve a content of up to 25.2% (wt).[39] In initial studies under benchtop laboratory conditions, it was decided to use the ionic liquid with known concentration of water. Karl Fisher titration measurements showed that the $BMIMBF_4$ used in these studies contained 7.5% (wt) water. The significance of water, deliberately added or present as an adventitious impurity in the ionic liquid, is considered later. The voltammetric behavior of TCNQ when dissolved in $BMIMBF_4$ is similar to that obtained in acetonitrile.[40,41] Thus, the steady-state voltammetry at a 2 μm diameter Pt microelectrode in the "wet" $BMIMBF_4$ (Figure 1a) exhibits two well-defined, sigmoidal-shaped one-electron reduction processes with half-wave potentials (approximately equal to the formal reversible potential $E_f^{0'}$) of −0.15 and −0.58 V vs $Fc^{0/+}$, respectively (eqs 2, 3):

$$TCNQ_{(BMIMBF_4)} + e^- \rightarrow TCNQ^-_{(BMIMBF_4)} \quad (2)$$

$$TCNQ^-_{(BMIMBF_4)} + e^- \rightarrow TCNQ^{2-}_{(BMIMBF_4)} \quad (3)$$

Analysis of the wave shape confirmed that both processes were fully reversible under these conditions. The diffusion coefficient of TCNQ, $D_{TCNQ} = 8.2 \times 10^{-8}$ cm^2 s^{-1}, in the "wet" $BMIMBF_4$ medium was calculated from the limiting current (i) obtained at the microelectrode and the relationship given in eq 4.[42]

$$i = 4nFrD_{TCNQ}C^*_{TCNQ} \quad (4)$$

where $n = 1$ is the number of electrons, r is the microelectrode radius (cm), D is the diffusion coefficient of TCNQ, c is the concentration (mol cm^{-3}), and other symbols have their usual

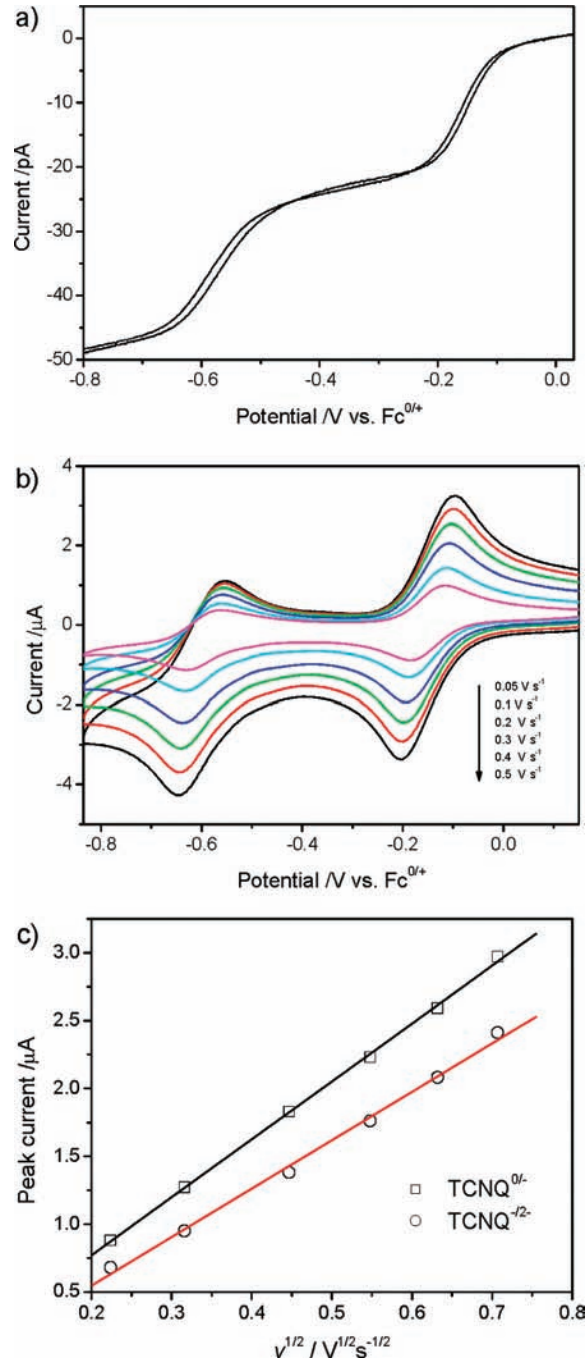

Figure 1. (a) Steady-state voltammogram obtained at a scan rate of 0.05 V s^{-1} at a 2 μm diameter Pt microdisc electrode for reduction of 5 mM TCNQ in "wet" $BMIMBF_4$; (b) transient voltammograms obtained at a glassy carbon marcodisc electrode over the scan rate range of 0.05−0.5 V s^{-1} for reduction of 4 mM TCNQ; and (c) dependence of the peak currents for the two reduction peaks of TCNQ in (b) on the square root of scan rate.

(38) Gritzner, G.; Kuta, J. *Pure Appl. Chem.* **1982**, *54*, 1527.
(39) Schroder, U.; Wadhawan, J. D.; Compton, R. G.; Marken, F.; Suarez, P. A. Z.; Consorti, C. S.; de Souza, R. F.; Dupont, J. *New J. Chem.* **2000**, *24*, 1009.
(40) Oyama, M.; Webster, R. D.; Suarez, M.; Marken, F.; Compton, R. G.; Okazaki, S. *J. Phys. Chem. B* **1998**, *102*, 6588.
(41) Bond, A. M.; Fletcher, S.; Symons, P. G. *Analyst* **1998**, *123*, 1891.
(42) Bard, A. J.; Faulkner, L. R. *Electrochemical Methods: Fundamentals and Applications*, 2nd ed.; Wiley: New York, 2001.

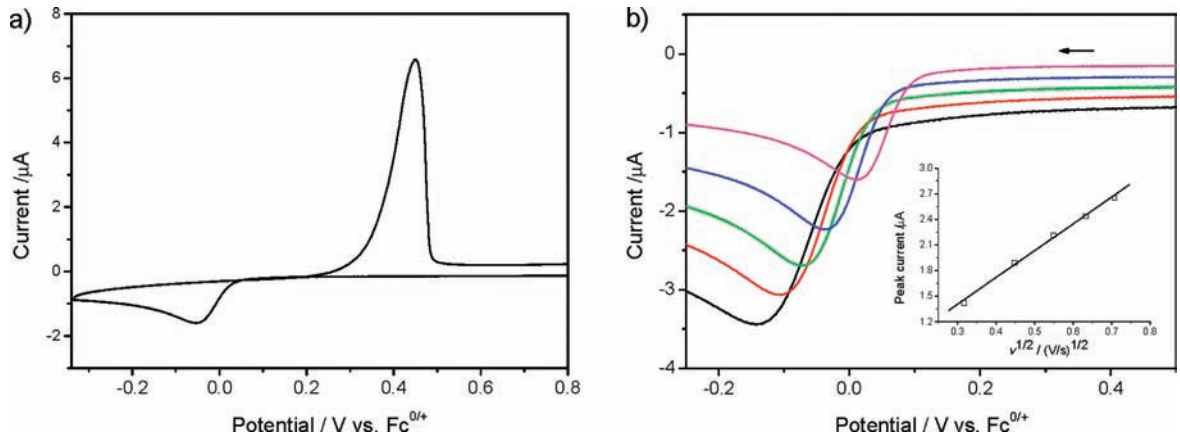

Figure 2. (a) Cyclic voltammogram obtained at a glassy carbon electrode for reduction of a 2.4 mM Ag^+ in "wet" $BMIMBF_4$ at a scan rate of 0.1 V s^{-1}; and (b) linear sweep voltammograms obtained over the scan rate range of 0.05−0.5 V s^{-1}, and the linear dependence (inset) of peak current on the square root of scan rate.

meanings. This value is much smaller than that obtained in an organic solvent such as acetonitrile (1.8×10^{-5} cm^2 s^{-1}),[40] as a result of much higher viscosity of $BMIMBF_4$ (34 cP for acetontrile versus 120 cP for the ionic liquid, 25 °C).[43,44] Transient voltammograms observed at a macrodisk GC electrode confirm that both processes are chemically reversible (Figure 1b). In the "wet" $BMIMBF_4$, the midpotentials calculated from the average of the reduction and oxidation peak potentials as −0.15 and −0.59 V are almost identical to the half-wave potentials detected under steady-state conditions. The peak potential separation for the first process increases from 63 to 106 mV when the scan rate is increased from 0.05 to 0.5 V s^{-1}. A similar increase is observed for the second process. This scan rate dependence may be associated with a small departure from reversibility at high scan rate but is mainly attributed to uncompensated *IR* (Ohmic) drop. The linear dependence of the TCNQ reduction peak currents on the square root of scan rate, $v^{1/2}$ (Figure 1c), indicates that both the $TCNQ^{0/-}$ and the $TCNQ^{-/2-}$ processes are diffusion-controlled.

2. Voltammetric Reduction of Ag^+ in "Wet" $BMIMBF_4$ in the Absence of TCNQ. A cyclic voltammogram obtained at 0.1 V s^{-1} for reduction of 2.4 mM Ag^+ at a glassy carbon electrode in the "wet" $BMIMBF_4$ exhibits a reduction peak at ca. −0.05 V (Figure 2a) on the cathodic scan. The reverse potential direction scan produces a current loop at 0.05 and 0.19 V indicative of a nucleation and growth mechanism for Ag deposition and a sharp stripping peak at 0.45 V. The pair of peaks is ascribed to the reductive deposition of Ag^+ (eq 5) onto the electrode surface and subsequent oxidative stripping of the silver (eq 6).

$$Ag^+_{(BMIMBF_4)} + e^- \rightarrow Ag_{(metal)} \quad (5)$$

$$Ag_{(metal)} \rightarrow Ag^+_{(BMIMBF_4)} + e^- \quad (6)$$

The Ag stripping peak currents are a function of the switching potential, but as expected are always higher than deposition peak currents. The charge ratio associated with each process, Q_a/Q_c, calculated from the integrated peak area, is always close to unity. The absence of underpotential deposition indicates minimal electro-deposited Ag−GC substrate interaction. The voltammetric behavior for Ag deposition at Pt and ITO is similar to that at the GC electrode.

Under conditions relevant to Figures 1 and 2, the Ag^+ reduction peak potential is about 140 mV more positive than that for TCNQ reduction. This difference from aqueous media and acetonitrile where values are similar is attributed to the modified thermodynamics available in the ionic liquid. In purely aqueous media and in acetonitrile, Ag^+ is strongly solvated. Therefore, the $Ag^{+/0}$ reduction process occurs at more positive potentials than in $BMIMBF_4$ where BF_4^- is only weakly coordinating. Clearly the 7.5% water in "wet" $BMIMBF_4$ does not play a strongly solvating role in the ionic liquid (see later). This lack of strong coordination of Ag^+ allows a potential separation between the $Ag^{+/0}$ and $TCNQ^{0/-}$ processes to occur in the ionic liquid.

The deposition peak potential shifts by 193 mV to more negative values when the scan rate is increased from 0.05 to 0.5 V s^{-1} (Figure 2b), as a consequence of the nucleation and growth process, uncompensated IR drop, and/or decrease in electrochemical reversibility. Nevertheless, a linear dependence of the Ag^+ reduction peak current, i_p, on $v^{1/2}$ indicates that reduction is controlled by diffusion (plot passes through the origin) at the peak potential. The diffusion coefficient for Ag^+, $D_{Ag^+} = 3.3 \times 10^{-7}$ cm^2 s^{-1}, was calculated from the slop of the relationship in eq 7, by assuming the process is fully irreversible with a charge transfer coefficient of 0.5, $n = n_a = 1$, and neglecting the electrode area change introduced by metallic silver deposition:

$$i_p = 3.01 \times 10^5 n(\alpha n_a)^{1/2} A D^{1/2}_{Ag^+} v^{1/2} C^*_{Ag^+} \ (T = 20\ °C) \quad (7)$$

This approximate value in "wet" $BMIMBF_4$ is slightly smaller than reported in $BMIMBF_4$ (4.2×10^{-7} cm^2 s^{-1}) by other workers at 25 °C,[45] but significantly smaller than in the less viscous $EMIMBF_4$ (6.0×10^{-7} cm^2 s^{-1}) at 25 °C[46] and aqueous electrolyte solution (2.6×10^{-5} cm^2 s^{-1} in 0.1 M KNO_3) at 25 °C.[45]

3. Voltammetric and Microscopic Investigation of Electrocrystallization Processes. 3.1. Voltammetric Reduction of Ag^+ in the Presence of TCNQ When the Concentration Ratio $[Ag^+]$: [TCNQ] < 1. Figure 3a shows a cyclic voltammogram obtained at a GC electrode over the potential range of −0.33 to 0.9 V

(43) Das, M.; Roy, M. N. *J. Chem. Eng. Data* **2006**, *51*, 2225.
(44) Shiddiky, M. J. A.; Torriero, A. A. J.; Zhao, C.; Burgar, I.; Kennedy, G.; Bond, A. M. *J. Am. Chem. Soc.* **2009**, *131*, 7976.

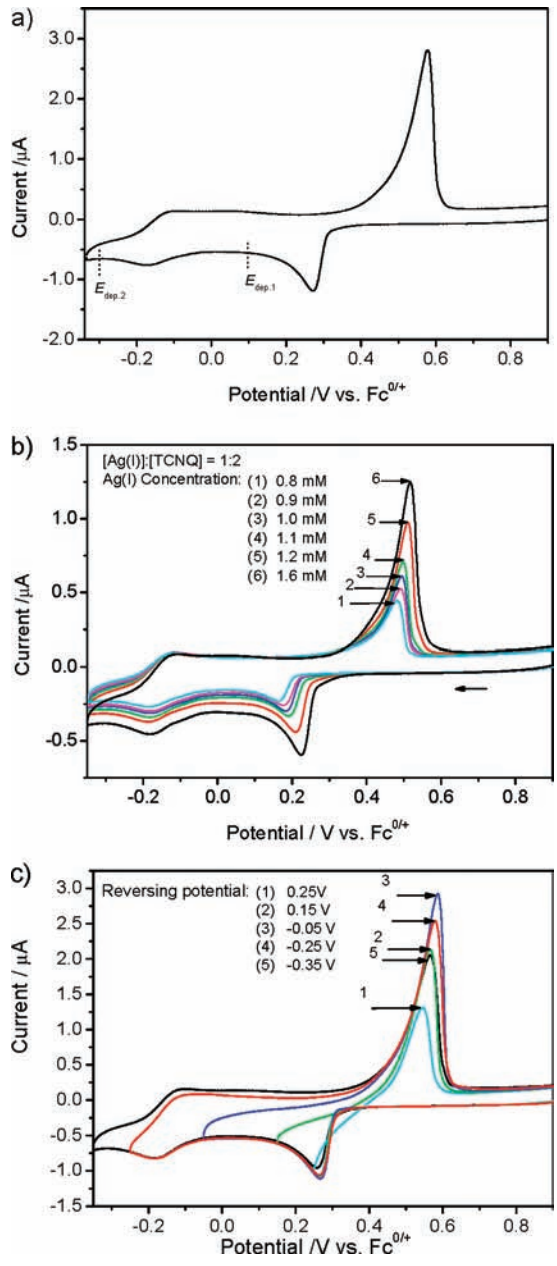

Figure 3. (a) Cyclic voltammogram obtained at 0.1 V s^{-1} in "wet" $BMIMBF_4$ containing 2.4 mM $Ag(MeCN)_4BF_4$ and 3.8 mM TCNQ with inset showing the linear dependence of reduction peak currents on the square root of scan rate; (b) cyclic voltammograms obtained at 0.05 V s^{-1} for different concentrations of $Ag(MeCN)_4BF_4$ and TCNQ at a constant ratio of 1:1.6 (Ag^+:TCNQ); and (c) cyclic voltammograms obtained at 0.1 V s^{-1} when the switching potentials are varied from 0.25 to −0.35 V.

when an Ag^+ salt is added to a TCNQ solution in "wet" $BMIMBF_4$ with $[Ag^+] < [TCNQ]$. Because it is the $TCNQ^{0/-}$ process that provides data of direct relevance to AgTCNQ formation, the second $TCNQ^{-/2-}$ process is not included in the voltammograms or the following discussion. Under these circumstances with a concentration ratio of $[Ag^+]:[TCNQ] = 1:1.6$ (2.4:3.8 mM), three well-defined processes ascribed to $Ag^{+/0}$, $TCNQ^{0/-}$ reduction, and an oxidative stripping process are detected with peak potentials of 0.27, −0.17, and 0.58 V vs $Fc^{0/+}$, respectively. Cyclic voltammetric data obtained as a function of scan rate under conditions of Figure 3a reveal that the reduction peak potential for reduction of Ag^+ shifts to more negative values by ca. 40 mV with increase of scan rate (0.01−0.1 V s^{-1}), while the peak potential associated with $TCNQ^{0/-}$ processes is nearly independent of scan rate. Furthermore, over this scan rate range, the peak currents for reduction of TCNQ and Ag^+ are found to be proportional to the square root of scan rate, $v^{1/2}$ (data not shown), indicating both processes are diffusion-controlled. Under these conditions, electrocrystallization of AgTCNQ will occur in the potential region between the two reduction processes, if electrodeposited Ag metal (eq 5) reacts with TCNQ on the voltammetric time scale (eq 8). AgTCNQ formed via this process could then be stripped off from the electrode when the potential is scanned in the reverse (positive) potential direction (eq 9).

$$Ag_{(metal)} + TCNQ_{(BMIMBF_4)} \rightarrow AgTCNQ_{(solid)} \quad (8)$$

$$AgTCNQ_{(solid)} \rightarrow Ag^+_{(metal)} + TCNQ_{(BMIMBF_4)} + e^- \quad (9)$$

The potential for reduction of TCNQ remains almost unchanged in the presence of Ag^+ (compare Figures 1 and 3). However, the Ag^+ reduction process, subsequently to AgTCNQ formation (eq 8), is shifted in positive potential direction by 340 mV relative to that for $Ag^{+/0}$ (compare Figures 2 and 3), resulting in a large peak potential separation of 440 mV between the Ag^+ and TCNQ processes. This large potential shift for Ag^+ reduction is predominantly attributed to the thermodynamics associated with the formation of solid AgTCNQ. Accordingly, the AgTCNQ oxidative stripping peak (eq 9), in comparison to the Ag stripping peak (eq 6), also is shifted in the positive direction by 130 mV under conditions relevant to Figures 2 and 3.

The concentration dependence of the electrocrystallization process with Ag^+ and TCNQ fixed at a ratio of 1:1.6 is shown in Figure 3b. With an increase in the Ag^+ concentration over the range of 0.8−1.6 mM, the peak potentials for Ag^+ reduction to form AgTCNQ and subsequent stripping peak for AgTCNQ shift in the positive direction by 60 and 34 mV, respectively. In contrast, the peak potential for $TCNQ^{0/-}$ process remains almost constant. The net effect is that the peak potential separation between two reduction processes ($\Delta E_p = E_{p,Ag^+} - E_{p,TCNQ^{0/-}}$) increases from 348 to 408 mV, which implies that deposition of Ag and subsequently formation of AgTCNQ is more favored thermodynamically at higher Ag^+ concentrations. Figure 3b, as expected, also shows that the peak currents for Ag^+ and TCNQ reduction increase linearly with Ag^+ and TCNQ concentrations, confirming that in this concentration range the formation of AgTCNQ occurs via eq 8.

The potential dependence of the electrocrystallization process in $BMIMBF_4$ containing 2.4 mM Ag^+ and 3.8 mM TCNQ is demonstrated in Figure 3c where the switching potential is varied from 0.25 to −0.35 V. When the switching potential is set at 0.25 V, the AgTCNQ oxidative stripping occurs at ca. 0.54 V, while the current loop detected under these conditions is indicative of a nucleation and growth process.[22] Extending the switching potential from 0.25 to −0.05 V progressively increases the stripping peak as more AgTCNQ is formed on the electrode surface during the time available on the negative direction potential scan. In contrast, when switching potential falls into TCNQ reduction region (−0.05 to −0.35 V), the current

(45) He, P.; Liu, H.; Li, Z.; Liu, Y.; Xu, X.; Li, J. *Langmuir* **2004**, *20*, 10260.
(46) Katayama, Y.; Dan, S.; Miura, T.; Kishi, T. *J. Electrochem. Soc.* **2001**, *148*, C102.

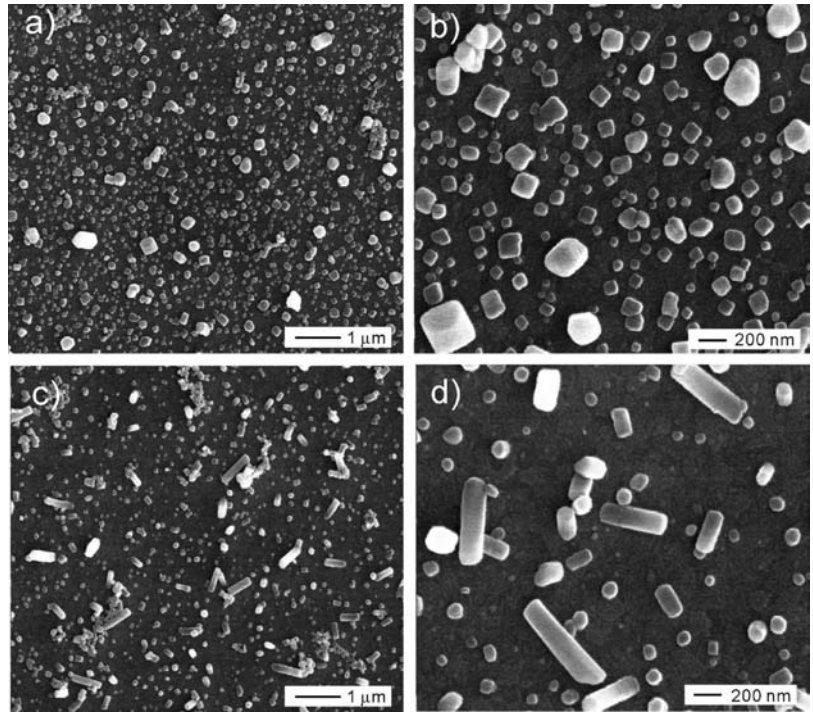

Figure 4. SEM images of AgTCNQ formed by electrocrystallization from "wet" $BMIMBF_4$ containing 2.4 mM $Ag(MeCN)_4BF_4$ and 4.8 mM TCNQ for 180 s onto an ITO electrode at a potential of (a,b) 0.1 V and (c,d) −0.3 V vs $Fc^{0/+}$.

magnitude for the stripping peak starts to decrease, indicating a decrease of AgTCNQ formed on electrode surface, as expected if the concentration of Ag^+ at the electrode surface is diminished by production of $TCNQ^-$. In this potential region, another route to form AgTCNQ becomes available, as illustrate in the reaction scheme (eq 10):

$$Ag^+_{(BMIMBF_4)} + TCNQ^-_{(BMIMBF_4)} \rightarrow AgTCNQ_{(solid)} \quad (10)$$

Controlled potential electrolysis at $E_{dep,1} = 0.1$ V for 180 s at an ITO electrode leads to deposition, by visual inspection, of a firmly attached blue film on the electrode surface. SEM images reveal the formation of well-separated, cube-shaped AgTCNQ nanostructures (Figure 4a,b). Inspection of images at higher magnification (Figure 4b) suggests that these nanocubes have grown outward after nucleation at well-separated defect sites present on the electrode surface, via a progressive nucleation−growth process. The widths of the AgTCNQ nanocubes formed generally lie in the range of 10−80 nm with some larger 300 nm ones being present. The smaller size of the AgTCNQ crystals, in comparison to those electrocrystallized from acetonitrile (>20 μm),[24] is attributed to the low values of the diffusion coefficients associated with the viscous ionic liquid and weaker Ostwald ripening. Controlled potential deposition at $E_{dep,2} = -0.3$ V gives rise to both nanoparticles and nanorods (Figure 4c,d). The diameters of the nanorods lie in the range of 40−150 nm with lengths up to 600 nm. The simultaneous formation of two morphologies of AgTCNQ may be associated with the simultaneous occurrence of two different electrocrystallization routes (eqs 5, 8 and 2, 10) in this potential region.

3.2. [Ag$^+$]:[TCNQ] = 1. When the Ag^+ concentration is increased, both the Ag^+ reduction and AgTCNQ stripping peak currents increase in magnitude and the peak potentials shift to more positive values (Figure 5a). Concomitantly, the peak current for the $TCNQ^{0/-}$ process decreases, becoming completely absent when the $[Ag^+] = [TCNQ]$ (Figure 5, curve 4). Electrocrystallization of AgTCNQ detected at a 2 μm diameter Pt microelectrode produces a sigmoidal-shaped near steady-state rather than transient behavior for the $Ag^{+/0}$ process. Upon scanning to more negative potentials, the $TCNQ^{0/-}$ process is not detected. On reversing the scan direction, current crossover is detected at 0.28 and 0.45 V, indicating the presence of a nucleation−growth mechanism. This is followed at more sufficiently positive potentials by a AgTCNQ stripping peak at ca. 0.5 V, similar to that found at a macro GC electrode. All of the data verify that formation of AgTCNQ occurs according to eqs 5 and 8 under these conditions. That is, Ag nanoparticles are deposited on electrode surface prior to reacting with TCNQ to form AgTCNQ, and if the Ag^+ concentration is high enough to consume all of the TCNQ at the electrode surface, no current associated with the $TCNQ^{0/-}$ process is observed.

Controlled potential electrolysis at $E_{dep,3} = 0.1$ V at an ITO electrode for 180 s now results in the formation of high-aspect ratio AgTCNQ nanorods (Figure 5c,d). The surface of these rods is smooth, and they have diameters in the range of 40−150 nm and lengths up to 1.5 μm.

3.3. [Ag$^+$]:[TCNQ] > 1. The presence of excess Ag^+ in a $BMIMBF_4$ solution of TCNQ leads to the detection of a new reduction process. Thus, cyclic voltammograms obtained at a scan rate of 0.1 V s^{-1} for the reduction of 6.5 mM Ag^+ in the presence of the 4.3 mM TCNQ at a GC electrode exhibit a sharp reduction process (labeled as P_{red} in Figure 6a) at the more negative potential of −0.06 V on the initial scan (shifts to more positive potentials on repetitive cycling of potential). On the reverse scan, a new stripping peak (labeled P_{strip}) is observed at 0.46 V. If the Ag^+ concentration is increased from 4.5 to 8.3 mM while maintaining a constant concentration ratio of $[Ag^+]$:$[TCNQ] = 1.5:1$, then peak potentials for Ag^+ reduction and stripping of AgTCNQ both shift to more positive values by 50 mV, the peak potential for P_{red} shifted in the negative directions

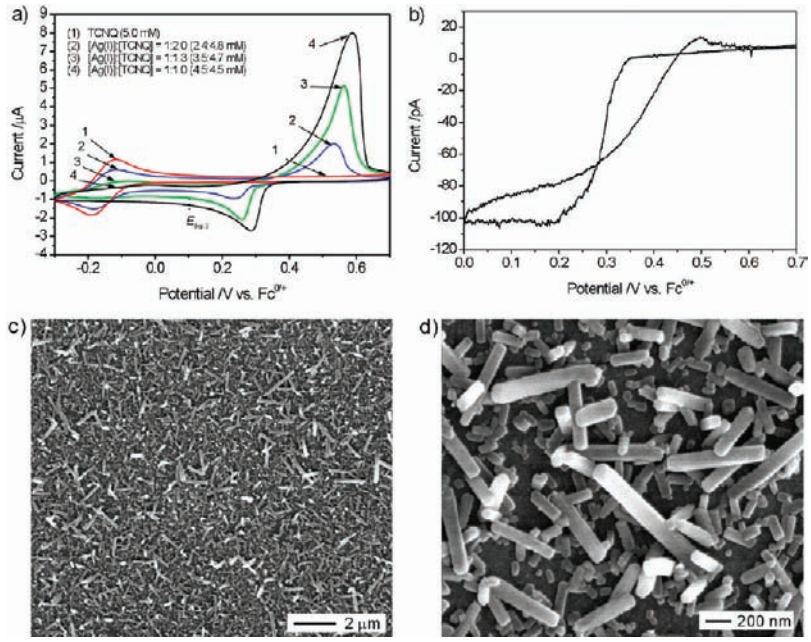

Figure 5. (a) Cyclic voltammograms obtained at a GC electrode at a scan rate of 0.1 V s^{-1} with stepwise addition of $Ag(MeCN)_4BF_4$ into a 5 mM TCNQ solution in "wet" $BMIMBF_4$ to give a final concentration ratio of 1:1. (b) Cyclic voltammogram obtained at a 2 μm diameter Pt microelectrode in the solution of (a). (c,d) SEM images of AgTCNQ formed by electrocrystallization for 180 s onto an ITO electrode at a potential of 0.1 V vs $Fc^{0/+}$.

by 40 mV, and P_{strip} shifts to more positive potentials by 75 mV (Figure 6b). The net effect is an increase in peak potential separation (ΔE_p) between the two reduction processes of 90 mV.

Shown in Figure 6c is the potential dependence of the two reduction processes. When the switching potential is 0.25 V, only one AgTCNQ oxidative stripping peak appears at ca. 0.45 V on the reverse scan, in accordance with eqs 5 and 8. When the switching potential is extended to encompass the P_{red} process region (<0.2 V), P_{strip} appears on the reverse scan and increases progressively as the switching potential become more negative. The results indicate that P_{red} process is also strongly potential dependent, and different forms of AgTCNQ are formed on the electrode surface. The current loop again detected also suggests the P_{red} process occurs via a nucleation−growth mechanism.

Electrocrystallization prior to the onset of P_{red} process at $E_{dep,4} = 0.2$ V for 180 s results in the deposition of more densely packed and longer nanowires (Figure 7a,b). At longer electrolysis times, ~300 s, SEM images (Figure 7c,d) reveal a compact film of much more densely packed, randomly oriented, and also larger crystals. Most of the bigger crystals exhibit outgrowth, and the cross sections of the wires have a quadrangular prism shape. More helical wires were observed at this longer electrolysis time, which is, as expected, due to the stronger influence of the lateral forces during the growth of crystals, as the nanowires are becoming more densely packed.

Distinctly different morphology is achieved when electrolysis is carried out at potential, $E_{dep,5} = -0.3$ V, which is more negative than for process P_{red}. A blue film derived from a mixture of short nanorods and nanoparticles is now formed (Figure 7e,f). Using an extended electrolysis time of 300 s (Figure 7g,h) produces a more uniform film. Higher magnification reveals that the nanorods and particles observed at shorter electrolysis time have been transformed to even smaller and more uniformly sized nanoparticles (40−170 nm). The formation of the nanocrystalline thin film via process P_{red} is attributed to the overpotential deposition of excess silver onto AgTCNQ crystals (rather than onto the bare electrode) and subsequent formation of AgTCNQ via eq 8.

4. Characterization of Electrocrystallized AgTCNQ by Elemental Analysis, Spectroscopy, and Powder XRD. AgTCNQ materials prepared on ITO electrode surfaces were examined by EDAX elemental analysis, which reveals that all of the electrocrystallized materials contain Ag, C, and N, as expected for AgTCNQ formation. Furthermore, spectroscopic and powder X-ray diffraction techniques were applied to establish the composition and phase of the crystals electrolyzed from $BMIMBF_4$.

4.1. Raman Spectroscopy. Figure 8a (1) contains the Raman spectrum of AgTCNQ nanowires electrocrystallized at a constant potential of 0.1 V for 300 s at an ITO electrode in "wet" $BMIMBF_4$ containing 6.5 mM $Ag(MeCN)_4BF_4$ and 4.3 mM TCNQ (see morphology in Figure 7c,d). The four characteristic principal vibration modes at 1205 cm^{-1} (C═CH bending), 1382 cm^{-1} (C−CN wing stretching), 1603 cm^{-1} (C═C stretching), and 2210 cm^{-1} (C−N stretching) confirm that the nanowires are AgTCNQ.[18] Comparison with the Raman spectrum of neutral TCNQ (Figure 8a (3)) reveals that the two principal vibration modes of TCNQ at 1455 cm^{-1} (C−CN wing stretching) and 2227 (C−N stretching) are red-shifted by 73 and 17 cm^{-1}, respectively, in AgTCNQ. The decrease in the vibrational energy is consistent with that obtained from other metal−TCNQ compounds and can be attributed to charge transfer between atomic Ag and free TCNQ, when TCNQ is reduced to $TCNQ^-$ to form AgTCNQ.[51] The Raman spectrum for the AgTCNQ thin film of nanoparticles (Figure 8a (2)) prepared when the deposition potential is more negative than the P_{red} process (−0.3 V) for 300 s (see morphology in Figure 7g,h) is indistinguishable from that found with AgTCNQ nanowires.

4.2. IR Spectroscopy. IR spectra recorded for AgTCNQ solid electrocrystallized on ITO electrode at potentials before or after

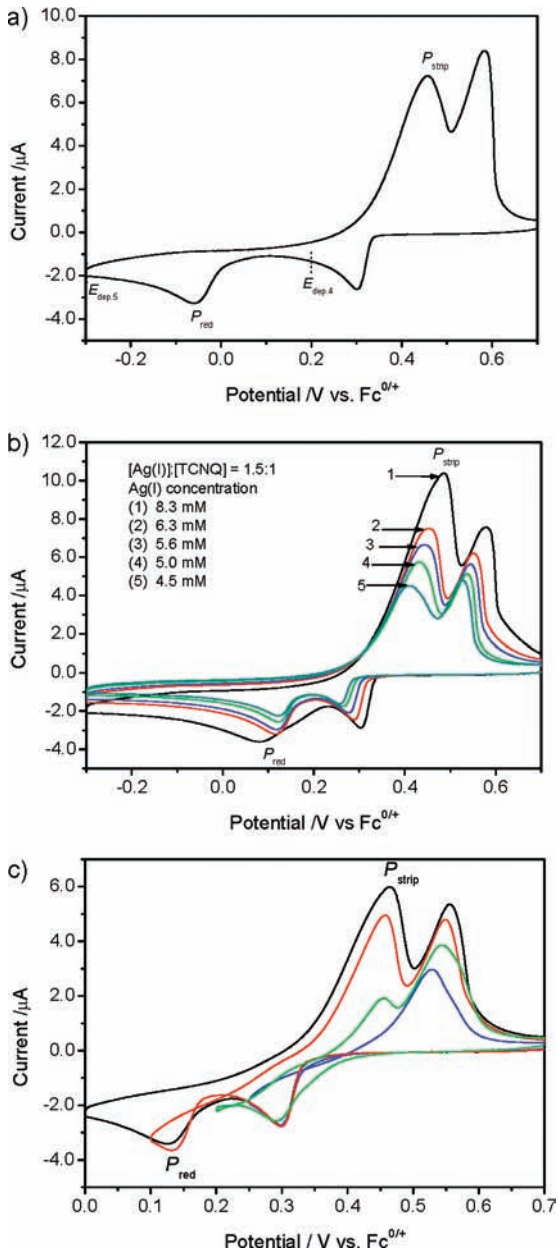

Figure 6. Cyclic voltammograms recorded at a GC electrode in a "wet" $BMIMBF_4$ solution containing (a) 6.5 mM $Ag(MeCN)_4BF_4$ and 4.3 mM TCNQ; (b) variable concentrations of $Ag(MeCN)_4BF_4$ and TCNQ but with a constant ratio of 1.5:1 (Ag^+:TCNQ); and (c) cyclic voltammograms obtained in solution (a) when the switching potential varies from 0.25 to 0 V. Scan rate = 0.1 V s^{-1} in (a), (b), and (c).

process P_{red} contain bands that also confirm the formation of AgTCNQ. Thus, the three strong bands observed in the υ(C′N) region at 2199, 2183, and 2160 cm^{-1}, a strong band observed in the υ(C═C) region at 1507 cm^{-1}, together with a δ(C−H stretching) band at 825 cm^{-1} are all indicative of the reduced $TCNQ^-$ anion radical, rather than $[TCNQ]^{2-}$, $[TCNQ-TCNQ]^{2-}$ dimer, or neutral TCNQ, and agree with IR data reported for AgTCNQ.[18] Thus, despite the fact that the two different pathways for eletrocrystallization produce different morphologies, AgTCNQ synthesized at potentials before and after process P_{red} exhibits indistinguishable IR spectra, implying they have the same phase.

4.3. Powder X-ray Diffraction. X-ray diffraction (XRD) patterns (Figure 8b) confirm that the electrocrystallized AgTCNQ is crystalline. Furthermore, diffraction peaks match those reported for AgTCNQ with an orthorhombic structure, where the Ag atom is coordinated to 4 N atoms in a distorted tetrahedral environment and TCNQ molecules stack face-to-face.[18] Adjacent TCNQ stacks are 90° relative to each other, and the two independent networks bring the TCNQ molecules together to form a columnar stack. Such structural feature leads to an enhanced conductivity along the stacks.[18] Therefore, AgTCNQ represents a quasi-one-dimensional material with high anisotropy, and the directional growth of AgTCNQ seeds is related to this structure feature. XRD powder patterns obtained for the AgTCNQ thin films also are indistinguishable from that for AgTCNQ nanowires (Figure 8b).

Raman, IR, and XRD data confirm the formation of AgTCNQ and also indicate that electrocrystallized AgTCNQ nanostuctures differ only in their morphology, but not in their phase.

5. Detection of Progressive Nucleation and Diffusion-Controlled Growth Mechanism by Chronoamperometry. Chronoamperometry provides access to information related to the type of nucleation and growth involved in an electrocrystallization process.[47−50] Figure 9a contains a family of current−time ($I-t$) transients for the deposition of AgTCNQ in "wet" $BMIMBF_4$ ionic liquid containing 6.5 mM $Ag(MeCN)_4BF_4$ and 4.3 mM TCNQ when the potential of a GC working electrode is progressively stepped from 0.6 V, where no faradic process occurs, to 0 V, which encompass potentials that are sufficiently negative to initiate the AgTCNQ deposition process. All transients exhibit a current maximum, which shifts at shorter times as the potential to which the electrode is stepped is made more negative. In all $I-t$ data, the capacitance current predominates at very short times before decaying exponentially. The faradic current, which becomes dominant at longer time, increases as the electroactive area increases, due to the growth of independent AgTCNQ crystals and/or the birth of new crystals. After reaching a maximum current value, the transients decrease at different rates, but finally merge into a common current−time profile at even longer times. This behavior is constant with the development and overlap of hemispherical diffusion zones around the growing nuclei, but which eventually coalesce to a planar electrode corresponding to linear diffusion. Stepping the potential to even more negative values relative to process P_{red} leads to detection of the well-known $t^{-1/2}$ (t = time) Cottrellian decay without any current maximum.[47,48] These $I-t$ data imply that the electrocrystallization of AgTCNQ is initiated by a nucleation process followed by a diffusion-controlled growth mechanism.

The early stages of an electrochemical reaction involving solid phase formation are usually associated with 2D and 3D nucleation processes.[47−50] Conformance to a theoretical model based on a 3D nucleation and diffusion-controlled growth is commonly found in the electrocrystallization of metal and semiconductors.[49,50] To determine whether the nucleation type is instantaneous or progressive, the current transients obtained for AgTCNQ deposition from $BMIMBF_4$ are presented in a nondimensional form using a normalized current (I^2/I_{max}^2, I_{max}= maximum current) versus time (t/t_{max}, t_{max} = time when I_{max} is

(47) Harrison, J. A.; Thirsk, H. R. In *Electroanalytical Chemistry*; Bard, A. J., Ed.; Dekker: New York, 1971; Vol. 5, p 67.
(48) Matthijs, E.; Langerock, S.; Michailova, E.; Heerman, L. *J. Electroanal. Chem.* **2004**, *570*, 123.
(49) Scharifker, B. R.; Hills, G. *Electrochim. Acta* **1983**, *28*, 879.
(50) Scharifker, B. R.; Mostany, J. *J. Electroanal. Chem.* **1984**, *177*, 13.
(51) Lewis, B.; Anderson, J. C. *Nucleation and Growth of Thin Films*; Academic Press: New York, 1978.

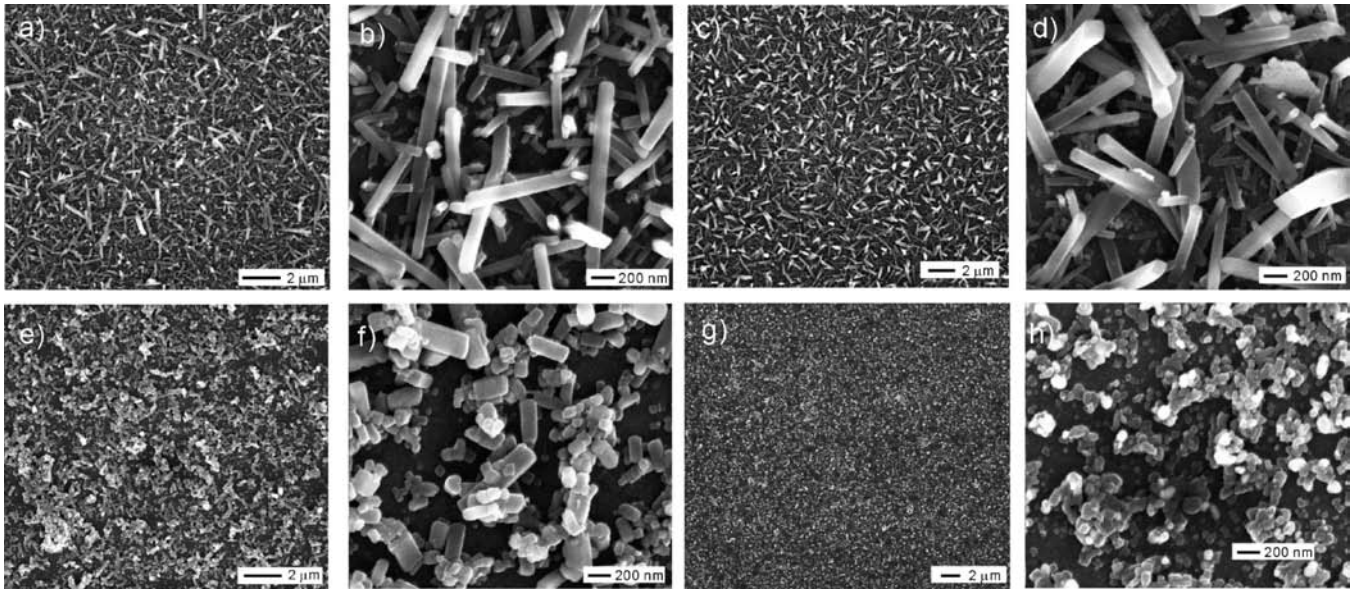

Figure 7. SEM images of AgTCNQ formed by electrocrystallization from "wet" $BMIMBF_4$ containing 6.5 mM $Ag(MeCN)_4BF_4$ and 4.3 mM TCNQ for (a,b,e,f) 180 s and (c,d,g,h) 300 s onto an ITO electrode at a potential of (a−d) 0.2 V and (e−h) −0.3 V vs $Fc^{0/+}$.

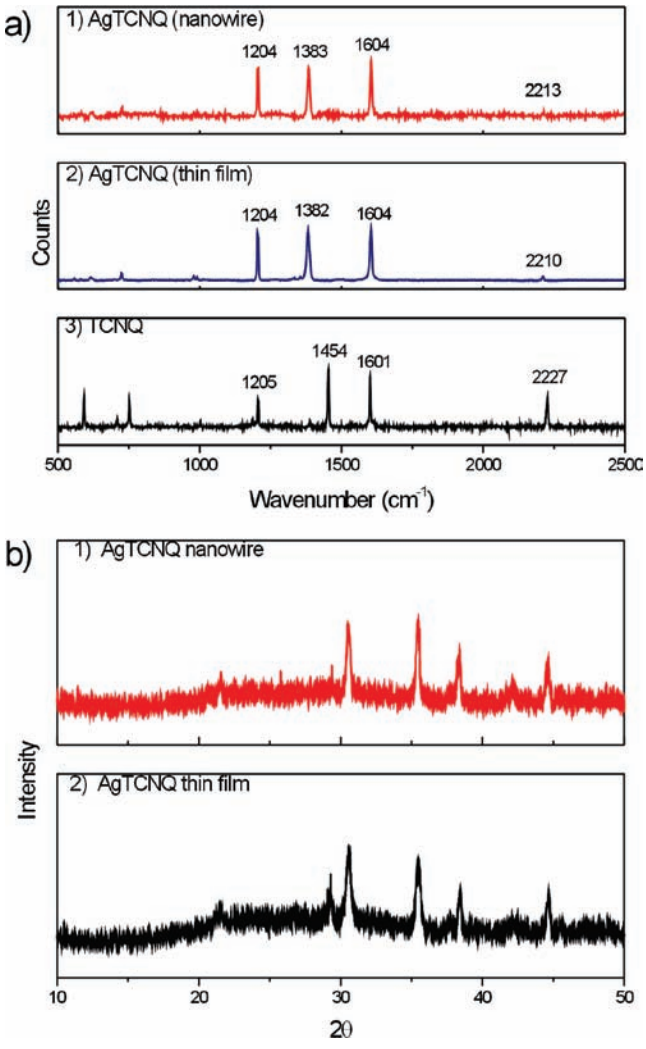

Figure 8. (a) Raman spectra derived from electrocrystallized (1) AgTCNQ nanowire, (2) a thin film of nanoparticles, and (3) solid TCNQ crystals; and (b) XRD pattern derived from electrocrystallized (1) AgTCNQ nanowires and (2) AgTCNQ thin film of nanoparticles.

obtained) plot, and data are compared to values derived theoretically using normalized growth laws.[49] Figure 9b contains a set of nondimensional experimental plots versus those predicted for the limiting cases of instantaneous and progressive 3D nucleation with diffusion-controlled growth. In all cases, experimental data match those derived from a progressive nucleation model. Therefore, electrocrystallization of AgTCNQ from $BMIMBF_4$ would appear to principally occur via a progressive nucleation and diffusion-controlled growth mechanism.

Scheme 1 illustrates the growth mechanism proposed for a single nanowire when the controlled potential allows Ag deposition but not TCNQ reduction. In this potential regime, Ag is first reduced and nucleated onto the well-separated defect sites of the electrode surface (Scheme 1a) according to an island (Volmer−Weber) growth model.[51] Dissolved AgTCNQ is simultaneously formed at the ionic liquid−solid interface upon diffusion and reaction with dissolved TCNQ. When AgTCNQ exceeds its solubility limit, AgTCNQ precipitates progressively onto the Ag seed, resulting in AgTCNQ stacking onto the existing interface to form a nanocube (Scheme 1b). This process requires less energy than forming a new nucleation site. Further growth of AgTCNQ is preferential in one (vertical) direction because AgTCNQ is highly anisotropic along the columnar stack of TCNQ (Scheme 1c). Consequently, single AgTCNQ nanowires grow longer and longer into the bulk solution until one of the reactants is depleted (Scheme 1d). Therefore, in the case of nanocubes and nanowires, the size of the AgTCNQ nanostructures produced via eqs 5 and 8 depends on the initial size of the Ag seeds and the supply of TCNQ, and hence on the concentration of Ag^+, TCNQ, and the electrolysis time. The final morphology is a result of competition between the diffusion of the solute and the anisotropy of growth. The growth of the AgTCNQ nanowires may be also affected by lateral stresses and interfacial tensions, which results in, for example, helical nanowires. Nanowires growth may also lead to congregation with nearby AgTCNQ nanowires, resulting in small variations in diameter and length.

6. Influence of Water. The presence of water in an ionic liquid is known to significantly influence physical properties

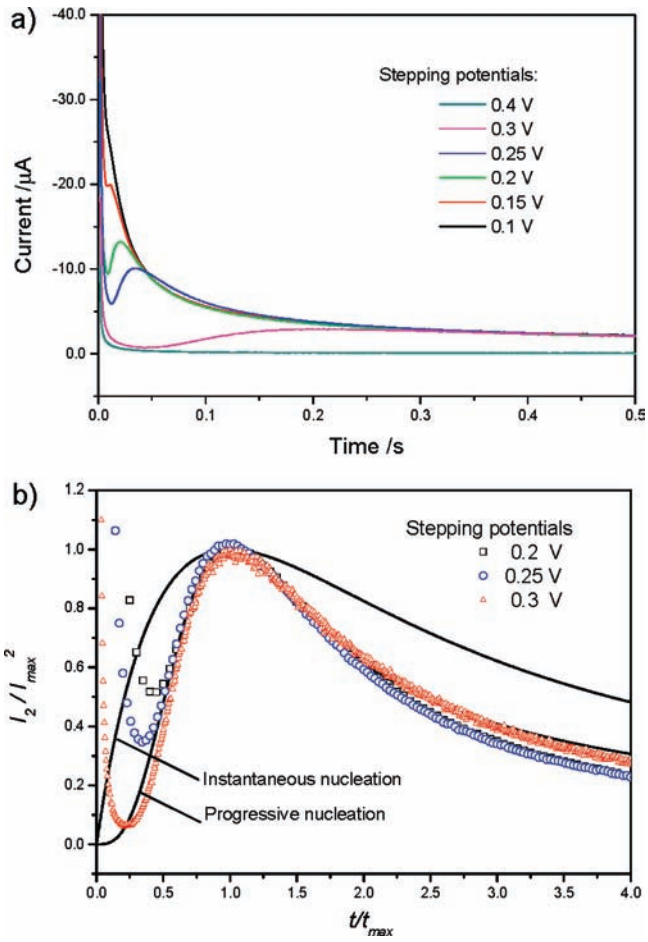

Figure 9. (a) Chronoamperometric current transients for the electrocrystallization of AgTCNQ onto a GC electrode in "wet" $BMIMBF_4$ solution containing 6.5 mM Ag^+ and 4.3 mM TCNQ; and (b) comparison of experimental data (dots) with theoretical (solid lines) based on the 3D instantaneous and progressive nucleation and diffusion-controlled growth process. The potential steps were all initiated at 0.6 V vs $Fc^{0/+}$.

Scheme 1. Schematic Illustration for the Mechanism for Electrocrystallization and Growth of a Single AgTCNQ Nanowire in Ionic Liquid[a]

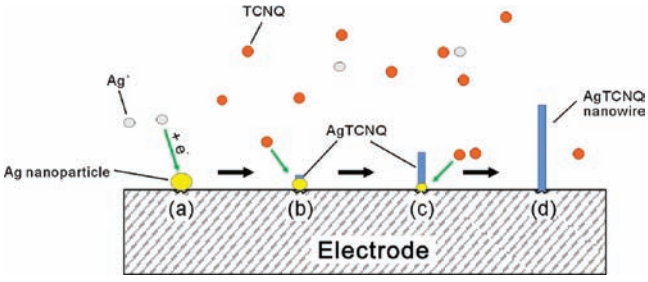

[a] (a) Reductive deposition of Ag nanoparticles at defect sites; (b) formation of AgTCNQ nuclei and nanocubes at solid−solution interface; (c) anisotropic growth along the columnar stack of TCNQ to form nanorods; and (d) further growth of single AgTCNQ nanowires until Ag is depleted.

such as viscosity, density, and surface tension,[39,52,53] and hence increase the diffusion coefficients of solutes. These changes in physical properties may affect the morphology of electrocrystallized materials. Water also may have a very different structure in ionic liquids relative to that in pure water or when present in molecular solvents. Spectroscopic studies show that at low water content in ionic liquids, water molecules tend to interact with the anion of the ionic liquid forming either a 1:1 type complex, H−O−H···anion, or a symmetric 1:2 type complex, anion···H−O−H···anion, but with the ionic network largely unperturbed. In most quaternary ammonium and imidazolium cation type ionic liquids (i.e., those lacking a classical hydrogen-bonding site), interaction with the cation is less significant.[54−56] At high concentration, water can disrupt or swell the ionic liquid network by formation and insertion of large water clusters, rather than single isolated water molecules.[54−56] Finally, with respect to metal ions, aquated cations such as $[Ag(H_2O)_x]^+$ may be formed. All of these modifications inevitably will alter the properties of the ionic liquid and the solutes contained therein and subsequently affect the electrocrystallization processes.

The influence of water on the voltammetric behavior in the hydrophilic $BMIMBF_4$ was initially studied by deliberately adding 0.45−15.9% (v/v) water to already "wet" $BMIMBF_4$ containing 7.5% (wt) water (determined by Karl Fisher titration method), 2.4 mM $Ag(MeCN)_4BF_4$, and 4.8 mM TCNQ. Upon addition of water in the above-mentioned range, the peak potential for reduction of Ag^+ shifts from 0.29 to 0.03 V and splits into two processes (Figure 10a). The AgTCNQ stripping peak also shifts negatively from 0.55 to 0.32 V. The negative shift in Ag^+ reduction and Ag stripping peak potentials indicate that the extent of solvation of the Ag^+ cation increases as the water concentration increases (presumably by formation of $[Ag(H_2O)_x]^+$ species). In contrast, the potential of the $TCNQ^{0/+}$ process is independent of added water, although the peak current values increase as the viscosity decreases.

An evaluation of the influence of water on the morphology of electrocrystallized AgTCNQ was conducted using "dried" $BMIMBF_4$ obtained by applying a vacuum at 20 °C at 0.03 mBar for 48 h to reduce the water content to ≤0.04%, and using $AgBF_4$, instead of $Ag(MeCN)_4BF_4$, as the source of Ag^+ ions. In the "dried" and acetonitrile-free ionic liquid solution, the diffusion coefficients calculated from the reduction peak currents obtained at a GC electrode inside a nitrogen-filled drybox and using the Randles−Sevcik relationship (eq 7) are 4.0×10^{-9} $cm^2\ s^{-1}$ for TCNQ and 7.7×10^{-8} $cm^2\ s^{-1}$ for Ag^+, respectively, which are much smaller than values of 8.2×10^{-8} and 3.3×10^{-7} $cm^2\ s^{-1}$ found in "wet" $BMIMBF_4$. Figure 10b,c shows SEM images of AgTCNQ electrocrystallized at 0.1 V vs $Fc^{0/+}$ onto an ITO electrode for 180 s from "dried" $BMIMBF_4$ (water content 0.04 wt %) containing equimolar (4.5 mM) TCNQ and $AgBF_4$. Formation of high-aspect ratio AgTCNQ nanowires is observed over the entire electrode area (Figure 10b). However, higher magnification images reveal the presence of small particles (typical diameters ca. 20−40 nm) among the nanowires (Figure 10c), which most commonly have a width of 20−40 nm, with ones up to 120 nm thick, and length of up to 700 nm. Obviously AgTCNQ nanostructures synthesized under the same electrochemical conditions from "wet" ionic liquid are much larger, which is mainly attributed to the smaller diffusion coefficients of TCNQ and Ag^+ in dry and more viscous

(52) Seddon, K. R.; Stark, A.; Torres, M. J. *Pure Appl. Chem.* **2000**, *72*, 2275.
(53) Huddleston, J. G.; Visser, A. E.; Reichert, W. M.; Willauer, H. D.; Broker, G. A.; Rogers, R. D. *Green Chem.* **2001**, *3*, 156.
(54) Cammarata, L.; Kazarian, S. G.; Salter, P. A.; Welton, T. *Phys. Chem. Chem. Phys.* **2001**, *3*, 5192.
(55) Koddermann, T.; Wertz, C.; Heintz, A.; Ludwig, R. *Angew. Chem., Int. Ed.* **2006**, *45*, 3697.
(56) Moreno, M.; Castiglione, F.; Mele, A.; Pasqui, C.; Raos, G. *J. Phys. Chem. B* **2008**, *112*, 7826.

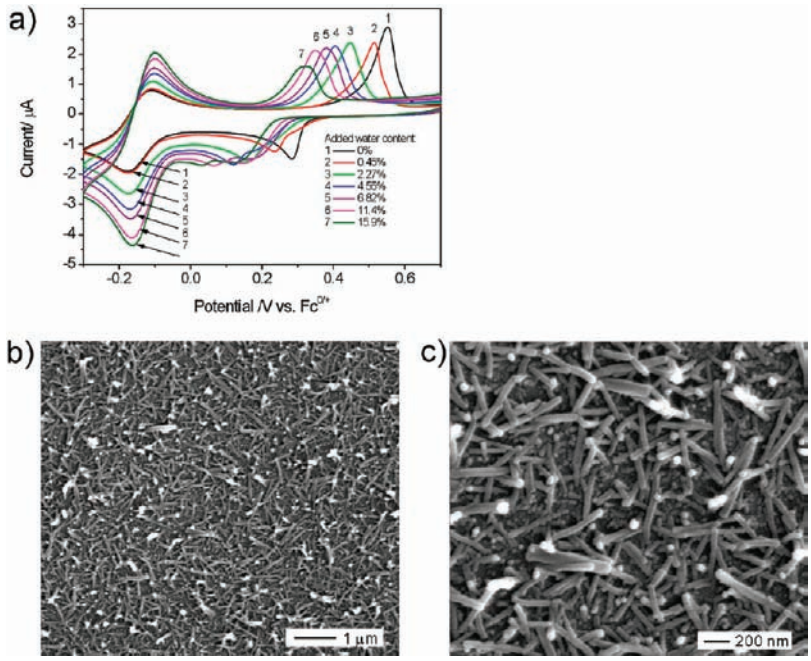

Figure 10. (a) Cyclic voltammograms obtained at scan rate of 0.1 V s^{-1} at a GC electrode upon addition of water (0−15.9% v/v) into a $BMIMBF_4$ solution containing 2.4 mM $Ag(MeCN)_4BF_4$ and 4.8 mM TCNQ, and (b,c) SEM images of AgTCNQ formed by electrocrystallization for 180 s onto an ITO electrode at a potential of 0.1 V vs $Fc^{0/+}$ from "dried" $BMIMBF_4$ solution containing 4.5 mM $AgBF_4$ and 4.5 mM TCNQ.

$BMIMBF_4$, which produces a slower growth process at the electrode surface and hence smaller structures. These data demonstrate that water present in ionic liquids as adventitious impurity can have an impact on the electrocrystallization process, but also that its deliberate presence provides a way of influencing the morphology of the nanostructures by changing the properties of the ionic liquid and the solutes.

Conclusions

Controlled electrocrystallization of AgTCNQ has been achieved from ionic liquid $BMIMBF_4$ via two distinctly different mechanisms. Voltammetric and microscopic investigations suggest that the electrocrystallization processes are strongly dependent on deposition potential, time, concentration, and stoichiometric ratio of Ag^+ and TCNQ, electrode material, and water content present in the ionic liquid. Application of spectroscopic and microscopic techniques confirms the structure, composition, and crystallinity of the electrocrystallized AgTCNQ and reveal that different nanostructures exhibit variability only in morphology but not phase or composition. The study highlights the capability of ionic liquids to act as a novel medium for electrocrystallization of technologically important materials, which are previously difficult to achieve in conventional organic solvents, and also paves an open way for the electrochemical fabrication of other metal−TCNQ charge transfer complexes with well-defined morphologies directly onto conducting or semiconducting electrode surfaces in a controlled manner as needed for applications related to nanoelectronic devices.

Acknowledgment. We are grateful to Mr. Geoff Burrell and Prof. Frances Separovic, School of Chemistry, Bio21 Institute, University of Melbourne, Australia, and Dr. Noel F. Dunlop, Orica Ltd., Melbourne, Australia, for useful discussions, and the Centre for Electron Microscopy, Monash University, for providing access to their SEM facilities. The study was financed by the Australian Research Council Linkage Grant LP0668123 and Orica Ltd., Australia.

JA9063519